Available online at www.sciencedirect.com
ScienceDirect
Magnetic Resonance Imaging xx (2010) xxx – xxx
MAGNETIC RESONANCE IMAGING

Exploring vision-related acupuncture point specificity with multivoxel pattern analysis

Linling Li[a], Wei Qin[a], Lijun Bai[a], Jie Tian[a,b,*]

[a]Life Science Research Center, School of Electronic Engineering, Xidian University, Xi'an 710071, China
[b]Institute of Automation, Chinese Academy of Sciences, Beijing 100190, China

Received 9 June 2009; revised 15 September 2009; accepted 27 November 2009

Abstract

Acupoint specificity is one of the central issues of functional magnetic resonance imaging (fMRI) studies of acupuncture and has been under discussed. However, strong and consistent proof has not been provided for the existence of acupoint specificity, and unsuitable analysis approach applied could be the reason. We observed that previous researches of acupoint specificity were mostly based on model-based methods which were limited to make exploration of acupoint specificity because of the inaccurate specified prior. Here we applied multi-voxel pattern analysis (MVPA) to investigate the specificity of brain activation patterns induced by acupuncture stimulations at a vision-related acupoint (GB37) and a nearby nonacupoint (NAP). Results showed that multiple brain areas could differentiate the central neural response patterns induced by acupuncture stimulation at these two sites with higher accuracy above the chance level. These regions included occipital cortex, limbic-cerebellar areas and somatosensory cortex. Our results support that the characteristic neural response patterns of brain cortex to the acupuncture stimulation at GB37 and a nearby NAP could differ from each other effectively with the application of MVPA approach.

Keywords: Acupuncture specificity; Functional magnetic resonance imaging, multi-voxel pattern analysis

1. Introduction

As a therapeutic measure, acupuncture is efficacious for various human disorders reported in clinical practice. According to the classical literatures of the traditional Chinese medicine, acupuncture actions embody a salient feature that acupuncture manipulation at certain points elicits specific effects over target organ systems which can be remote from the needling sites. However, the acupoint specificity is still a controversial research topic. In order to prove the existence of acupoint specificity, previous researches have focused on the relationship between acupuncture needle stimulations at vision-related acupoints and their corresponding cortical activation patterns. A seminal study has reported that acupuncture manipulation at vision-related acupoints induced specific fMRI signal changes in the occipital cortex, which did not exist in sham group [1]. A group of following studies focused on the specificity of vision-related acupoints likewise [2–4]. One of them argued that acupuncture stimulation at a vision-related acupuncture point (GB37) did not directly produce activation in the visual cortex and associated areas [5]. But lately, another research, aiming to compare brain activation changes in the occipital lobe by stimulating two vision-related Traditional Chinese Medicine (TCM) acupoints and a nonacupoint (NAP), observed that the acupuncture stimulation at both vision-related acupoints and the NAP produced similar widespread fMRI signal deactivations [6]. This result did not support the specificity of vision-related acupoints.

Previous fMRI activation studies, which were based on a block paradigm design, mostly applied general linear model (GLM) approach to detect acupuncture effects according to a presumable temporal pattern of brain activation induced by acupuncture administration [7–9]. GLM approach is well suited for testing whether variability in a voxel's time course can be explained by a set of predefined regressors that model predicted responses to stimulus (such as acupuncture).

* Corresponding author. Institute of Automation, Chinese Academy of Sciences P.O. Box 2728, Beijing 100190, China. Tel.: +86 010 82618465; fax: +86 010 62527995.
E-mail addresses: tian@ieee.org, tian@fingerpass.net.cn (J. Tian).

0730-725X/$ – see front matter © 2010 Elsevier Inc. All rights reserved.
doi:10.1016/j.mri.2009.11.009

However, this model-dependent approach is not valid in cases when limited or no prior temporal information is available, for example, it does not work efficiently testing the acute effects of a new drug or food intake on the brain [10]. According to the theory of TCM, acupuncture induces long lasting post-manipulation effects [11]. This fact brings about that the actual temporal information for acupuncture-induced changes in brain remains unclear. Therefore, GLM approach is not optimal for the study of acupuncture effects when the precise timing and duration of physiological events cannot be specified a prior. And the statistical inferences derived from GLM estimates are limited. Other approaches which are free of any statistical inferences on the temporal profile of the neutral responses to acupuncture stimulation should be introduced to explore the central neutral response. Recently, multivoxel pattern analysis (MVPA) has drew much attention as an alternative approach to classical analysis methods of functional mapping [12–14]. MVPA, with data-driven nature, are free of any hypothesis on the temporal profile of the event, and could be more appropriate to investigate the subtle differences between acupuncture performed at different points.

In this study, we applied MVPA to analyze the difference of neutral response patterns induced by acupuncture stimulation at GB37 and one of its nearby NAP. We hypothesized that neuroimaging findings derived from MVPA could identify subtle differences of neural responses following acupuncture stimulation at a vision-related acupoint and a prefixed NAP.

2. Materials and methods

2.1. Subjects

Twenty-two Chinese healthy college students gave their written consents and participated in the present study (11 males and 11 females, ages of 21.4±1.8, right-handed). The protocol was approved by the West China Hospital Subcommittee on Human studies and conducted in accordance with the Declaration of Helsinki. None of the participants have previous acupuncture experience or had been exposed to a high magnetic field.

2.2. Acupuncture experiment procedures

Subjects were divided into two groups in a semirandomized order: of them 11 subjects received acupuncture stimulation performed at GB 37 on the mid-shin which is widely used as treatment for vision-related disorders [15] (a manual acupuncture condition, ACUP group) and the other 11 subjects received sham stimulation at a NAP, a nonmeridian-point (a sham acupuncture condition, SHAM group).

In each ACUP run or SHAM run, the participant underwent a conventional block of acupuncture stimulation at GB 37 or nearby NAP. The experimental paradigm used during the fMRI scan was an ON/OFF block design. Each block run consisted of a baseline scanning of 1 min at the beginning, two stimulation epochs of 30 s which were separated by an interval period of 50 s and followed by a resting period of 50 s.

2.3. fMRI scanning procedure

Subjects were scanned in a 3.0-T Signa (Siemens) MR whole body Scanner. A foam pillow and a band (across the forehead) were used to restrict head movement. Functional images were collected in a sagittal orientation parallel to the AC-PC plane with 5 mm slice thickness (no gaps) using a single shot gradient-recalled echo planar imaging (EPI) sequence. The EPI pulse sequence had the following parameters: TE=30 ms, TR=2000 ms, flip angle=90°; matrix size=64×64, field of view 240×240 mm^2, giving an in-plane resolution=3.75×3.75 mm. The scan covered the entire brain including the cerebellum and brainstem.

At the end of each ACUP or SHAM run, the participant was questioned about deqi sensations (i.e., sensations of aching, tingling, fullness, cool, warm, sharp pain and dull pain). The sensation rates from 0 to 10 (0=no sensation, 1–3=mild, 4−6=moderate, 7–8=strong, 9=severe and 10=unbearable sensation).

2.4. fMRI data analysis

2.4.1. Preprocessing

For each subject, 110 functional volumes (totally 220 s) were acquired in each run and the first 5 volumes of each run were removed to eliminate nonequilibrium effects of magnetization. Data preprocess were done with SPM5 (Wellcome Department of Imaging Neuroscience, London, UK). All scans were realigned to remove residential motion effects, spatial normalized on the MNI space, and then resample at 3×3×3 mm. No spatial smoothing was applied because this conventional preprocessing step may remove fine-grained spatial information which could be useful for pattern recognition analysis of MVPA.

2.4.2. Multi-voxel pattern analysis

The preprocessed fMRI data were used to form an basic MVPA research which is a straightforward application of pattern classification techniques [12]. The performance of pattern recognition application typically depends a great deal on the step of feature selection which determines the number and quality of the variables (i.e., features) that are given to the classifier. So an efficient feature selection step needs to be able to abstract a subset or composite set of features which contains enough information to perform the classification but not so many to degrade classifier performance. In this study, a novel variant of the "searchlight" approach [16] was applied to select an appropriate set of voxels in order to define multivariate features as the input of pattern classification analysis. We defined a spherical multivariate "searchlight" centered on each voxel in turn to combine the signals from all voxels

falling into it, and this "searchlight" was moved through the whole brain cortex. Therefore this multivariate feature selection method can evaluate sets of voxels based on the informativeness of blood oxygenation level dependent (BOLD) signal changes over those voxels [12]. The classification performance of each voxel shows how well the multivariate signal in the local spherical neighborhood differentiated the experimental conditions.

In detail, we first defined a small spherical cluster with 6-mm radius which comprised 33 voxels (according to the "searchlight" with optimal or near-optimal detection performance [16]) of 3-mm width in each dimension for a given voxel v_i. We extracted the unsmoothed preprocessed fMRI data for each voxel in the fixed local cluster to yield a feature vector for this central voxel v_i, and a single feature in it was defined by x_{tj} which was the signal of a voxel j at a given time point t. Therefore, we acquired a data matrix $X=T\times V$ where T was the number of time points of each run and V was the number of the voxels in this spherical cluster. We then applied singular value decomposition (SVD) as a dimension reduction device to reduce the raw data matrix to its eigenvectors and only the major singular vector which spanned the greatest variance seen in the data was chosen to define the final feature vector for each run of each subject (a description of SVD can be found in Appendix A).

Previous machine learning related studies have developed an enormous range of classification algorithms that can be applied in MVPA studies [17]. Here, the classification was performed with the support vector machines (SVM). SVM is based on the statistical learning theory [18] and has been acknowledged as a powerful tool for statistical pattern recognition [19]. A brief summary of its essential concepts can be found in Appendix B. SVMs have been successfully used in multiple MVPA fMRI studies and, especially, have much better performance when large numbers of dimensions were used [20]. The classification was performed with the LIBSVM implementation (http://www.csie.ntu.edu.tw/wcjlin/libsvm). The SVM classifier is trained by providing examples of the form $<x,y>$ where x represents a spatial pattern, here in our case is the final feature vector of each subject, and y is the class label (y=1 for ACUP group and y=−1 for SHAM-group). We evaluated the performance of the classifier using the leave-one-subject-out cross validation test. The proposed approach here had K-folds where K (equals 22) is the number of all the subjects involved. For each fold, we assigned the features of the K-1 subjects obtained from the "searchlight" centered on voxel v_i to a "training" data set that was used to train this linear classifier. And then, the class label of the central voxel v_i belonged to the other subject ("test" data) was predicted by classifying its feature vector using the trained classifier. In total, the training and test procedures were repeated 22 times, each with feature vectors of N-1 different runs/subjects assigned as training data set and feature vector of one different run/subject assigned as test data set. The classifier accuracy was measured by the proportion of runs correctly classified for central voxel v_i. Therefore, average classifier accuracy was yielded for v_i by averaging all the accuracies achieved for every fold of this K-fold cross-validation procedure. Then, the same procedure was repeated for the next spatial position at v_i, and the classifier accuracy for each voxel was then used to create a three-dimensional spatial map of classifier accuracy for each position v_i to illustrate the discriminating areas in the whole brain cortex.

2.4.3. GLM-based analysis

Besides MVPA, we have performed fMRI data analysis with the application of voxel-wise GLM approach to both groups. The statistical analysis was performed subsequently at both individual level and group level using the same preprocessed fMRI data set which had been analyzed with MVPA. In the individual analysis, one t-contrast was defined as stimulation phase minus resting phase in both two groups. Each of the resulting statistical maps indicated the voxel-wise signal changes for a particular stimulation condition relative to the baseline of resting. These maps from each subject of these two groups were then used to calculate two-sample t test in SPM5. Statistical analysis was done with a threshold at $P<.005$ (uncorrected).

3. Results

3.1. Psychophysical responses

The prevalence of these deqi sensations reported by all the subjects was expressed as the percentage of individuals in the group that reported the given sensations (Fig. 1A). A statistical analysis found no difference between the ACUP group and SHAM group in regard to the prevalence of these sensations (paired t test, $P>.05$). However, differences did exist in terms of several types of sensations. Aching (ACUP group: 58% of subjects; SHAM group: 33%), fullness (ACUP group: 58%; SHAM group: 42%), and Dull pain (ACUP group: 17%; SHAM group: 0) was found greater for ACUP group. Tingling (ACUP group: 33%; SHAM group: 50%) was found greater for SHAM group. The intensity of sensations was expressed as the averaged score±S.E. (Fig. 1B). The levels of sensations were kept low (mild to moderate), and no significant differences occurred in the average sensation intensity between the ACUP group and SHAM group. There was also no significant difference in the MASS indexes (a weighted average of all sensations using an exponential smoothing) between these two conditions (paired t test, $P>.05$) [21].

3.2. Discriminating results of MVPA

We trained and tested the classifier to distinguish the patterns of neural responses elicited by acupuncture stimulations performed at one vision-related acupoint and one NAP. Table 1 summarized the brain areas with significant discriminating accuracies higher than the threshold of discriminating level (65%, higher than the

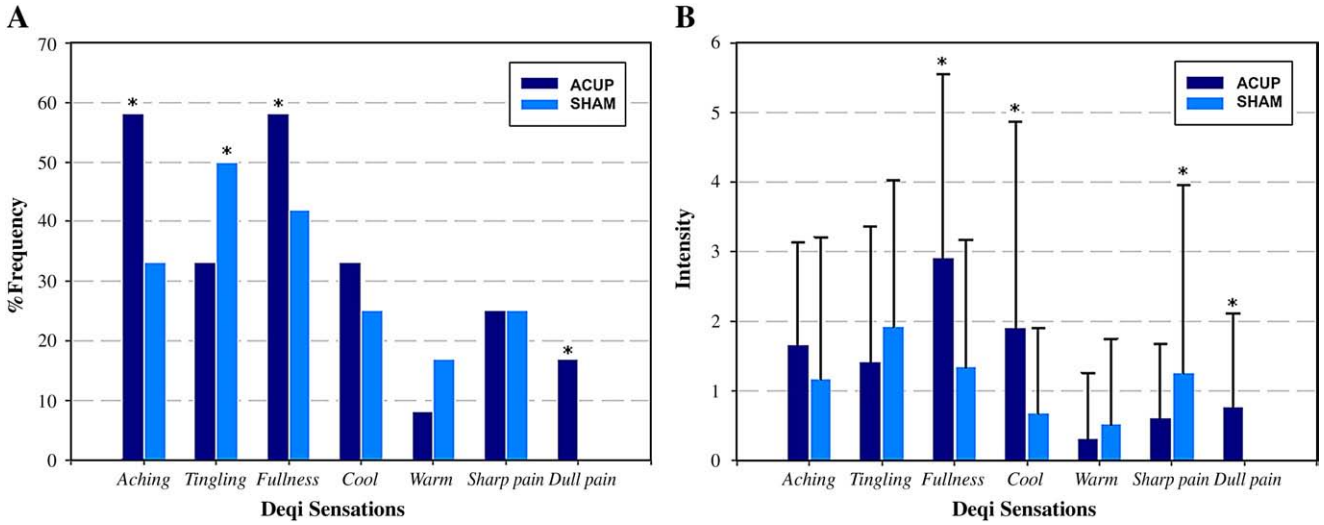

Fig. 1. Results of psychophysical analysis. (A) A percentage of subjects who reported having experienced the given sensation. Sensations of aching, fullness, and dull pain were found more prevalent for ACUP group. Tingling was found more prevalent for SHAM group. (B) The intensity of the reported sensations measured by an averaged score (with standard error bars) on a scale from 0 denoting no sensation to 10 denoting an unbearable sensation. Sensations of fullness, cool and dull pain were found greater for ACUP group. Sharp pain was found greatest for SHAM group.

chance level 50% which has been applied as the threshold of classification accuracy in previous studies [22–23]). Spatial maps with classifier accuracies were shown in Fig. 2. Subregions of vision-related cortex showed strong discriminating ability to distinguish the neural response patterns elicited by acupuncture stimulations performed at different sites, including inferior occipital gyrus (IOG), bilateral lingual gyrus (LG) (Fig. 2A and B), middle occipital gyrus (MOG) and fusiform gyrus (FG). The resulting discriminating map also displayed high accuracies in some major structures of limbic-cerebellar system, including the insula (C), rostral anterior cingulate cortex (rACC) (D) and perigenual anterior cingulate cortex (pACC) (E), pons (F) amygdala (G) and culmem in anterior lobe (H) and declive of vermis (I) in posterior lobe of cerebellum. In addition, small region of somatosensory cortex (secondary somatosensory cortex, SII) (J) was also identified with high discriminating accuracies.

3.3. Results of two-sample t test based on GLM approach

Group analysis averaged across all subjects and sessions identified no region where fMRI signals increased above threshold when calculating the contrast of acupuncture

Table 1
Significant discriminating accuracies derived from pattern classification between ACUP and SHAM (with 0.65 as threshold of discriminating accuracy)

		Talairach			DA	*n*			Talairach			DA	*N*
		x	*y*	*z*					*x*	*y*	*z*		
Limbic system					0.72		Sensorimotor						
Amygdala	R	21	−7	−15	0.86	5	SII	L					
PH/Hipp	L	−18	−47	−5	0.77	30		R	65	−20	15	0.82	5
	R	24	−47	−10		14	Occipital cortex						
dACC	L				0.82		Cuneus	L	−3	−67	9	0.91	53
BA 24/32	R	6	33	18	0.77	10	BA17	R	21	−83	37	0.82	49
pACC	L	−6	32	−4	0.95	21	IOG/LG	L	−6	−64	3	0.82	17
BA24/32	R	6	38	−2	0.95	54	BA18	R	21	−97	−8	0.86	46
MCC/PCC	L	−6	−42	33	0.82	47	MOG/FG	L	−24	−89	21	0.82	36
BA 32/23	R	9	−45	38	0.82	38	BA19	R	27	−94	−13	0.82	26
Insula	L	−48	−34	18	0.82	15	Cerebellum						
BA13	R	42	−43	19	0.82	9	Culmen	L	0	−59	−7	0.91	124
Brainstem								R	24	−42	−16	0.95	153
Pons	L	−18	−33	−29	0.95	63	Declive	L	−6	−56	−12	0.86	50
	R	6	−27	−21	0.82	36		R	42	−68	−22	0.95	101

BA, brodmann area; PH, parahippocampus; Hipp, hippocampus; dACC, dorsal cingulate cortex; MCC, middle cingulate cortex; PCC, posterior cingulate cortex; SII, secondary somatosensory cortex; DA, discriminating accuracy; *N*, the number of voxels identified.
The discriminating accuracies showed in this table were the highest value among all the N voxels identified (with accuracy higher than 0.65) for the specific brain areas.

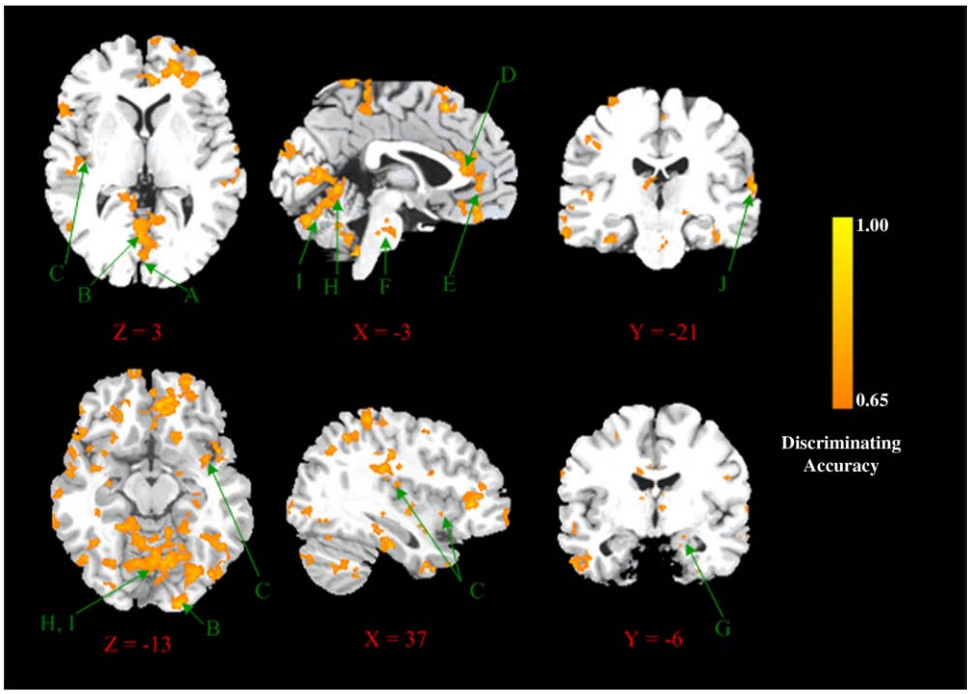

Fig. 2. Resulting spatial maps with accuracies for discriminating neural response patterns between real acupuncture stimuli at GB37 and the sham acupuncture. (A and B) Lingual gyrus. C, left insula; D, rostral anterior cingulate cortex; E, perigenual anterior cingulate cortex; F, pons; G, amygdala; H, culmen in the anterior lobe of cerebellum. I, declive of vermis in posterior lobe of cerebellum. J, secondary somatosensory cortex.

greater than baseline in the occipital lobe. And response patterns of brain cortex were similar for ACUP and NAP. The results of two-sample *t* test were summarized in the Table 2. It shows activations existing in small areas of inferior occipital gyrus and lingual gyrus in the occipital lobe. This indicates that occipital lobe deactivation patterns between these two points do not significantly differ in spite of minor differences in fMRI signal change. Besides, a few of brain areas showed activations in the result of two-sample *t* test which indicated stronger averaged neutral responses to acupuncture stimulation of ACUP group compared with SHAM-group, including some major structures of limbic-

Table 2
Significant changes in signal intensity derived from ACUP group versus SHAM group (two-sample *t* test, T=2.85, P<.005, uncorrected)

		Talairach			*t*	N			Talairach			*t*	*N*
		x	*y*	*z*					*x*	*y*	*z*		
Limbic system							Temporal cortex						
PH	L						BA 37/39	L	−36	−60	28	3.27	3
BA 30/36	R	30	−38	−8	3.76	6		R	45	−67	9	3.24	3
MCC/PCC	L						Parietal cortex						
BA 24	R	12	−10	39	3.14	5	IPC/precuneus	L	−48	−28	24	4.11	9
Insula	L	−45	−34	21	3.41	3		R	42	−45	38	3.64	5
BA13	R	42	0	−5	4.75	4	Occipital cortex						
Subcortical							Cuneus	L	−3	−77	29	3.30	5
Thalamus	L	−12	−26	1	3.52	4	BA18	R					
	R	15	−20	15	3.61	3	IOG/LG	L	−36	−79	−4	3.26	4
Brainstem							BA19	R					
Pons	L	−15	−27	−21	3.33	2	Cerebellum						
	R	9	−22	−24	3.09	2	Culmen	L	−6	−47	2	3.38	9
Sensorimotor								R	36	−45	−20	3.37	10
SI	L	−48	−27	40	3.84	8	Declive	L	−27	−59	−15	3.82	17
	R							R					
SMA	L												
BA 6	R	3	−3	53	3.10	3							

SI, primary somatosensory cortex; SMA, supplementary motor area; IPC, inferior parietal cortex.
The *t* values showed in this table were the highest *t* value among all the *N* voxels identified and considered significant at P<.005 for the specific brain areas.

cerebellar system and small regions of primary somatosensory cortex and supplementary motor area.

4. Discussion

We applied MVPA to explore the acupoint specificity by identifying the subtle difference in the neural response patterns induced by acupuncture stimulations at one vision-related acupoint and one nearby NAP. We found that indeed several brain areas predicted whether the subject was currently receiving acupuncture stimulation at the GB37 or the NAP with high accuracies. These most discriminating areas include subregions of occipital cortex, the limbic-cerebellar system, and somatosensory cortex.

It has been reported that acupuncture performed at vision-related acupoints and NAP both evoked BOLD signal changes in occipital cortex, and their neural response patterns had multiple overlapped regions, which did not significantly differ from each other in fMRI signal change [6]. In our study, we proved that by applying MVPA, the subtle difference in BOLD signal changes in subregions of occipital cortex could be extracted to distinguish the different neural response patterns. The highest discriminating accuracy in left cuneus of occipital gyrus reached 91%. Besides, there were also several regions of lingual gyrus, middle occipital gyrus and fusiform gyrus where discriminating accuracy was lower but still above 65% (threshold of discriminating level). The results supported that the neutral response patterns in occipital cortex induced by acupuncture stimulation at ACUP and NAP could be distinguished effectively.

High discriminating accuracies were also achieved in multiple regions of limbic-cerebellar system (shown in Fig. 2), including insula, rACC and pACC, pons, amygdala, culmem in anterior lobe and declive of vermis in posterior lobe of cerebellum. The limbic-cerebellar system plays a central role in regulating and integrating sensorimotor, autonomic, endocrine and immunological functions, as well as cognition and affect. Furthermore, acupuncture-performed at main classical acupoints involves brain circuits that regulate and integrate diverse somatic and mental functions in a coordinated manner. Therefore, the limbic-cerebellar system's central role in this multifaceted effects of acupuncture stimulation is not surprising and has been affirmed in a former study [7]. Here, our results identified subregions of the limbic-cerebellar system could distinguish the verum acupuncture from the sham acupuncture condition based on the differences of fMRI signal changes. We came to the conclusion that verum acupuncture exerted different modulation over the limbic-cerebellar system compared with sham acupuncture.

Results showed that a subregion of SII presented discriminating accuracies up to 82%. Both verum and sham acupuncture stimulus with the same needling manipulation induce signal responses located in SII which is generally involved in the nociceptive processing and pain perception [24]. However, our result here presented the identified subregions of SII which could discriminate different acupuncture stimulations performed at ACUP and NAP with high accuracies. This substantiates that SII played different role in the neutral responses to acupuncture stimulation at real acupoint and NAP in sensory-discriminative aspects.

For comparison, standard GLM analysis was also conducted in our study. The two-sample t test ($P<.005$, uncorrected), ACUP group versus SHAM group, showed activations in similar brain areas, including subregions of limbic-cerebellar system and occipital cortex, as the brain areas with high discriminating accuracies derived from MVPA. These activations demonstrate that acupuncture stimulation performed at real acupoint aroused larger signal changes in some brain regions. However, these activations showed in the Table 2 are generally small even the result of two-sample t test were uncorrected with a threshold $P<.005$. Therefore, the neutral response patterns of acupuncture stimulation at ACUP and NAP had multiple overlapping regions and did not significantly differ from each other. This result is in consistent with previous study [6]. But the MVPA approach identified large distribution of brain areas which presented discriminating accuracies higher than 65%. Compared to GLM-based approach, this illuminated that the discrepancies of spatial patterns derived from MVPA approach could present the differences of neutral responses to acupuncture between the ACUP and SHAM groups with high statistical reliability.

Before closing, several potential limitations of our study must be addressed. One limitation is the feature selection approach we used. In order to consider the dependency among voxels, we applied "searchlight" method where the correlation structure among a local set of voxels in a "searchlight" is utilized. This method relies on the assumption that the discriminating information could be provided in neighboring voxels within a "searchlight" of specified radius. However, this locally distributed analysis might be sub-optimal when no hypothesis is available on the size of the neighborhood and might fail to detect the discriminative patterns jointly encoded by distant regions [23]. The second limitation exists in the step of dimension reduction. We applied SVD as a dimension reduction device and simply allowed SVM to work with the first singular vectors which had the largest corresponding singular value. There was indeed loss of information in this step. Future researches will employ more efficient feature selection strategies prior to the pattern recognition analysis in order to reduce the dimensionality with little loss of information and to preserve sensitivity to small effects. The third limitation is that the relatively small sample size involved in the pattern recognition analysis. It is suggested that a sufficient sample size and number of repeated scans across same subject is necessary to ensure sample power to detect changes in brain activity associated with a task and avoid the

"overfitting" problem in pattern classification problem [25–26]. In our study, we only acquired one functional run for each subject follow the acupuncture stimulation at GB 37 or NAP. So the sample size was not quite large enough for pattern recognition analysis and this factor might slightly reduce the statistical effectiveness of our results derived from MVPA.

5. Conclusion

This is the first attempt applying multi-voxel pattern analysis to explore the acupoint specificity with basic pattern recognition approach. We observed that high discriminating accuracies were achieved in subregions of vision-related cortex, limbic-cerebellar system, and somatosensory cortex. These discriminating areas indicate the distinct BOLD signal changes induced by verum acupuncture stimulation performed at GB37 compared with one nearby NAP. Therefore, our study could provide positive evidence into the acupuncture specificity.

Acknowledgments

This paper is supported by Changjiang Scholars and Innovative Research Team in University PCSIRT under Grant No.IRT0645, Chair Professors of Cheung Kong Scholars Program, CAS Hundred Talents Program, the Joint Research Fund for Overseas Chinese Young Scholars under Grant No.30528027, the National Natural Science Foundation of China under Grant No. 30873462, 90209008, 30870685, 30672690, 30600151, 60532050, 60621001, the Beijing Natural Science Fund under Grant No. 4071003, the Project for the National Key Basic Research and Development Program (973) under Grant No.2006CB705700, and 863 program under Grant No. 2008AA01Z411.

Appendix A. Singular value decomposition

In linear algebra, the SVD is an important factorization of a rectangular real or complex matrix, with several applications in signal processing and statistics. Applications which employ the SVD include computing the pseudoinverse, least squares fitting of data, matrix approximation and determining the rank, range and null space of a matrix.

Suppose M is an m-by-n matrix whose entries come from the field K, which is either the field of real numbers or the field of complex numbers. Then there exists a factorization of the form: $M=U\sum V^T$, where U is an m-by-m unitary matrix over K, the matrix $\sum$ is m-by-n diagonal matrix with nonnegative real numbers on the diagonal, and V^T denotes the conjugate transpose of V, an n-by-n unitary matrix over K. Such a factorization is called a singular-value decomposition of M.

A common convention is to order the diagonal entries $\sum_{i,i}$ in nonincreasing fashion. In this case, the diagonal matrix $\sum$ is uniquely determined by M (though the matrices U and V are not). The diagonal entries of $\sum$ are known as the singular values of M.

Appendix B. Support vector machine

The SVM algorithm will be briefly summarized here [18]. It has been shown that the optimal hyperplane is defined as the one with the maximal margin of separation between the two classes. There is a weight vector $\boldsymbol{w}$ and an offset b such that

$$y_i\left[(\boldsymbol{w})^T\boldsymbol{v}_i + b\right] > 0 \tag{B.1}$$

where y_i is the class label (+1 for the class 1 and −1 for the class 2), and $\boldsymbol{w}_i$ are the training examples (projected volumes onto the principal components).

Rescaling $\boldsymbol{w}$ and b such that the point(s) closest to the hyperplane satisfy

$$\left|(\boldsymbol{w})\boldsymbol{v}_i + b\right| = 1 \tag{B.2}$$

Obtains the canonical form of the hyperplane, given by

$$y_i\left((\boldsymbol{w})^T\boldsymbol{v}_i + b\right) \geq 1 \tag{B.3}$$

The margin, the distance to a separating hyperplane from the point closer to it, measured perpendicularly to the hyperplane is $1/\|\boldsymbol{w}\|^2$. To maximize the margin, one has to minimize $\|\boldsymbol{w}\|$ subject to Eq. (B.3). The solution $\boldsymbol{w}$ is constructed by solving a constrained quadratic optimization problem, and it has an expansion in terms of a subset of training examples that lie on the margin (support vectors), given by

$$\boldsymbol{w} = \sum_{i=1}^{N} \alpha_i \boldsymbol{y}_i \boldsymbol{v}_i \tag{B.4}$$

The training examples $\boldsymbol{v}_i$ with coefficients α_i nonzero, called support vectors, carry all information relevant about the classification problem.

The class label of a test example $\boldsymbol{v}$ is computed by the hyperplane decision function, given by

$$f(\boldsymbol{v}) = \operatorname{sgn}\left(\sum_{i=1}^{N} y_i\alpha_i\left(\boldsymbol{v}^T\boldsymbol{v}_i\right) + b\right) \tag{B.5}$$

References

[1] Cho ZH, Chung SC, Jones JP, Park JB, Park HJ, Lee HJ, et al. New findings of the correlation between acupoints and corresponding brain cortices using functional MRI. Proc Natl Acad Sci U S A 1998;95:2670–3.

[2] Li G, Cheung RT, Ma QY, Yang ES. Visual cortical activations on fMRI upon stimulation of the vision-implicated acupoints. Neuroreport 2003;14:669–73.
[3] Litscher G, Rachbauer D, Ropele S, Wang L, Schikora D, Fazekas F, et al. Acupuncture using laser needles modulates brain function: first evidence from functional transcranial Doppler sonography and functional magnetic resonance imaging. Lasers Med Sci 2004;19: 6–11.
[4] Parrish TB, Schaeffer A, Catanese M, Rogel MJ. Functional magnetic resonance imaging of real and sham acupuncture. IEEE Eng Med Biol Mag 2005;24:35–40.
[5] Gareus IK, Lacour M, Schulte AC, Hennig J. Is there a BOLD response of the visual cortex on stimulation of the vision-related acupoint GB 37? J Magn Reson Imaging 2002;15:227–32.
[6] Kong J, Kaptchuk TJ, Webb JM, Kong JT, Sasaki Y, Polich GR, et al. Functional neuroanatomical investigation of vision-related acupuncture point specificity — a multisession fMRI study. Hum Brain Mapp 2009;30:38–46.
[7] Hui KKS, Liu J, Marina O, Napadow V, Haselgrove C, Kwong KK, et al. The integrated response of the human cerebro-cerebellar and limbic systems to acupuncture stimulation at ST 36 as evidenced by fMRI. Neuroimage 2005;27:479–96.
[8] Hui KK, Liu J, Makris N, Gollub RL, Chen AJ, Moore CI, et al. Acupuncture modulates the limbic system and subcortical gray structures of the human brain: evidence from fMRI studies in normal subjects. Hum Brain Mapp 2000;9:13–25.
[9] Wu MT, Sheen JM, Chuang KH, Yang P, Chin SL, Tsai CY, et al. Neuronal specificity of acupuncture response: a fMRI study with electroacupuncture. Neuroimage 2002;16:1028–37.
[10] Liu Y, Gao JH, Liu HL, Fox PT. The temporal response of the brain after eating revealed by functional MRI. Nature 2000;405: 1058–62.
[11] Beijing S. Nanjing colleges of traditional. Chinese medicine Essentials of Chinese acupuncture. Beijing: Foreign Language Press; 1980.
[12] Norman KA, Polyn SM, Detre GJ, Haxby JV. Beyond mind-reading: multi-voxel pattern analysis of fMRI data. Trends Cogn Sci 2006;10: 424–30.
[13] Haynes JD, Sakai K, Rees G, Gilbert S, Frith C, Passingham RE. Reading hidden intentions in the human brain. Curr Biol 2007;17: 323–8.
[14] Mourão-Miranda J, Friston KJ, Brammer M. Dynamic discrimination analysis: a spatial–temporal SVM. Neuroimage 2007;36:88–99.
[15] Lade A. Acupuncture points: images and functions. Seattle: Eastland Press; 1989.
[16] Kriegeskorte N, Goebel R, Bandettini P. Information-based functional brain mapping. Proc Natl Acad Sci U S A 2006;103:3863–8.
[17] Duda RO, Hart PE, Stork DG. Pattern classification. New York: Wiley; 2001.
[18] Vapnik V. The nature of statistical learning theory. Springer-Verlag; 1995.
[19] Boser BE, Guyon IM, Vapnik VN. A training algorithm for optimal margin classifiers. Proceedings of the 5th Annual ACM Workshop on Computational Learning Theory. Pittsburgh, PA. New York: ACM; 1992. p. 144–52.
[20] Mitchell TM, Hutchinson R, Niculescu RS, Pereira F, Wang X, Just M, et al. Learning to decode cognitive states from brain images. Machine Learning 2004;57:145–75.
[21] Kong J, Gollub R, Huang T, Polich G, Napadow V, Hui K, et al. Acupuncture de qi, from qualitative history to quantitative measurement. J Altern Complement Med 2007;13:1059–70.
[22] Cox DD, Savoy RL. Functional magnetic resonance imaging (fMRI) "brain reading": detecting and classifying distributed patterns of fMRI activity in human visual cortex. Neuroimage 2003;19:261–70.
[23] De Martino F, Valente G, Staeren N, Ashburner J, Goebel R, Formisano E. Combining multivariate voxel selection and support vector machines for mapping and classification of fMRI spatial patterns. Neuroimage 2008;43:44–58.
[24] Tracey I, Mantyh PW. The cerebral signature for pain perception and its modulation. Neuron 2007;55:91.
[25] Huettel SA, Song AW, McCarthy G. Functional magnetic resonance imaging. Sunderland (MA): Sinauer Associates, Inc.; 2004.
[26] Chen X, Pereira F, Lee W, Strother S, Mitchell T. Exploring predictive and reproducible modeling with the single-subject FIAC dataset. Hum Brain Mapp 2006;27:452–61.